Check for updates

Calcium/calmodulin inhibition of the *Arabidopsis* BRASSINOSTEROID-INSENSITIVE 1 receptor kinase provides a possible link between calcium and brassinosteroid signalling

Man-Ho OH*, Hyoung Seok KIM*, Xia WU*, Steven D. CLOUSE†, Raymond E. ZIELINSKI* and Steven C. HUBER*‡[1]

*Department of Plant Biology, University of Illinois, Urbana, IL 61801, U.S.A., †Department of Horticultural Science, NC State University, Raleigh, NC 27695, U.S.A., and ‡U.S. Department of Agriculture, Agricultural Research Service, Urbana, IL 61801, U.S.A.

The receptor kinase BRI1 (BRASSINOSTEROID-INSENSITIVE 1) is a key component in BR (brassinosteroid) perception and signal transduction, and has a broad impact on plant growth and development. In the present study, we demonstrate that *Arabidopsis* CaM (calmodulin) binds to the recombinant cytoplasmic domain of BRI1 in a Ca^{2+}-dependent manner *in vitro*. *In silico* analysis predicted binding to Helix E of the BRI1 kinase subdomain VIa and a synthetic peptide based on this sequence interacted with Ca^{2+}/CaM. Co-expression of CaM with the cytoplasmic domain of BRI1 in *Escherichia coli* strongly reduced autophosphorylation of BRI1, in particular on tyrosine residues, and also reduced the BRI1-mediated

transphosphorylation of *E. coli* proteins on tyrosine, threonine and presumably serine residues. Several isoforms of CaM and CMLs (CaM-like proteins) were more effective (AtCaM6, AtCaM7 and AtCML8, where At is *Arabidopsis thaliana*) than others (AtCaM2, AtCaM4 and AtCML11) when co-expressed with BRI1 in *E. coli*. These results establish a novel assay for recombinant BRI1 transphosphorylation activity and collectively uncover a possible new link between Ca^{2+} and BR signalling.

Key words: brassinosteroid, BRASSINOSTEROID-INSENSITIVE 1 receptor kinase, calcium signalling, signal transduction, transphosphorylation, tyrosine autophosphorylation.

INTRODUCTION

Plants contain a large family of RLKs (receptor-like kinases) that regulate various growth and developmental processes, phytohormone perception, and biotic and abiotic stress responses [1–3]. BRs (brassinosteroids) are essential plant steroid hormones that regulate multiple aspects of plant growth and development through a complex signal transduction pathway [4]. BR signalling is mediated by the BR receptor, BRI1 (BRASSINOSTEROID-INSENSITIVE 1) [5], and its co-receptor BAK1 (BRI1-ASSOCIATED KINASE 1) [6], both of which belong to the LRR (leucine-rich repeat) RLK family [7]. These plant RLKs contain an LRR extracellular domain, a single-pass transmembrane domain and a cytoplasmic domain that consists of a protein kinase domain flanked by a juxtamembrane and a C-terminal domain. BR signal transduction is initiated by the perception of the hormone in the extracellular domain of the BRI1 receptor kinase [8,9], which then binds to BAK1, with the result that the kinase domains activate by auto- and trans-phosphorylation of residues in the RLK cytoplasmic domains [10–14]. The signal is then transduced via intracellular kinases that phosphorylate downstream transcription factors that alter the expression of genes involved in cell elongation, division and differentiation [6,15,16]. Although the plant RLKs are classified as serine/threonine protein kinases, previous results show that BRI1 and BAK1 also autophosphorylate on tyrosine residues and are thus dual-specificity kinases [11,17]. Site-directed mutagenesis of specific tyrosine residues in BRI1 [11,18] and BAK1 [17] followed by *in vitro* biochemical analysis and an *in vivo* test demonstrated

that tyrosine autophosphorylation plays an important role in plant receptor kinase function and is an important component in BR signalling.

Ca^{2+} is a universal second messenger that acts as a mediator of stimulus–response coupling in eukaryotes. In plants, various abiotic and biotic stimuli, including phytohormones, mechanical and oxidative stresses, and microbial elicitors, trigger changes in intracellular Ca^{2+} concentration [19,20]. CaM (calmodulin) is one of the primary Ca^{2+}-sensor proteins that can transduce cytosolic Ca^{2+} changes into a cellular response. CaM has no enzymatic activity, but functions by changing its conformation in the presence of Ca^{2+} and concomitantly binding and altering the activities of a wide array of target proteins [21,22]. Identification and characterization of the physiologically relevant protein targets of CaM is particularly important to understand how these proteins have a role in translating Ca^{2+} signals into cellular responses. In terms of BR signalling, previous studies have identified one enzyme involved in BR biosynthesis as a Ca^{2+}/CaM-regulated enzyme [23]. Interestingly, whereas several RLKs have also been reported as binding targets of CaM [24,25], BRI1 was reported to not interact with CaM *in vitro* when expressed as the recombinant cytoplasmic domain [25]. Curiously, even when binding of CaM to the recombinant receptor kinase cytoplasmic domains was shown to occur, no changes in kinase activities were found, and thus the functional significance of CaM–RLK interactions remains unclear.

In the present study, we show that the cytoplasmic domain of BRI1 interacts with CaM *in vitro* in a Ca^{2+}-dependent manner. A high-probability CaM-binding site in BRI1 was predicted to

occur in subdomain VIa of the kinase domain using an algorithm based on known binding proteins (http://calcium.uhnres.utoronto.ca/ctdb/ctdb/home.html), and a synthetic peptide corresponding to the predicted CaM-binding domain was found to interact with CaM *in vitro*. We also report the novel result that co-expression of CaM with BRI1 in *Escherichia coli* specifically inhibited the kinase activity of BRI1. Both autophosphorylation of BRI1 and BRI1-mediated transphosphorylation of *E. coli* proteins (which is established as a new assay for BRI1 kinase activity) were inhibited. Differences between CaM isoforms were observed, suggesting specificity in the response. Our results suggest that Ca^{2+}/CaM may attenuate the kinase activity of BRI1 and thereby uncover a possible new link between Ca^{2+} and BR signalling.

EXPERIMENTAL

Materials

Synthetic peptides with an N-terminal biotin group were produced by GenScript and were >90% pure: W980, LNWSTRRKI-AIGSARGLAF; W1099, LVGWVKQHAKLRISDVFD.

Pull-down assays

For pull-down experiments, His_6–AtCaM7 (At is *Arabidopsis thaliana*) proteins (1 μg) immobilized on 150 μl of Ni-NTA (Ni^{2+}-nitrilotriacetate)–agarose beads (Qiagen) were incubated with FLAG-tagged recombinant BRI1 protein (1 μg) in 20 mM Mops (pH 7.5), 1 mM DTT (dithiothreitol) and protease inhibitor mixture {4 mM NaF, 0.2 mM AEBSF [4-(2-aminoethyl)benzenesulfonyl fluoride], 0.2 mM benzamidine, 0.2 mM caproic acid and 0.4 μM E-64} for 1 h at 4°C with or without the addition of 100 μM $CaCl_2$. The agarose beads were washed twice with a buffer of 5 mM sodium phosphate and 150 mM NaCl (pH 7.4), and then twice with the binding buffer. Proteins were eluted using SDS/PAGE loading buffer by heating for 5 min at 95°C. The initial supernatant and the eluted proteins were loaded in equal volumes on to SDS/12% polyacrylamide gels, and immunoblots were performed with the FLAG-tag-specific antibodies. Pull-down assays using neutravidin-coated agarose beads (Pierce) and biotinylated synthetic peptides were conducted using the same buffer and reaction conditions as indicated. Briefly, the biotinylated synthetic peptides (BRI1 W980) containing the putative CaM-binding site of BRI1 were immobilized on neutravidin–agarose beads, and then incubated with the His_6–AtCaM7 protein. FLAG–BRI1 protein bound to the beads was eluted using sample buffer and detected by immunoblotting with anti-His_6 antibodies.

Homology modelling of BRI1 kinase domain

The homology structure of the BRI1 kinase domain (residues 883–1158) was obtained with MODELLER (http://www.salilab.org/modeller/), based on templates of tomato protein kinase Pto (PDB code 2QKW, ~38% identity) and human IRAK-4 (interleukin-1-receptor-associated kinase 4) (PDB code 2NRU, ~34% identity). Structural alignment and visualization were performed using visual molecular dynamics [26].

Protein-interaction studies

CaM binding to FLAG–BRI1 was measured using SPR (surface plasmon resonance) with a Biacore™ 3000 system (GE Healthcare). A total of 300 RU (response units) of the His_6–AtCaM7 protein was immobilized on to an Ni-NTA sensorchip.

Six concentrations of recombinant BRI1 protein were individually passed over the sensorchip in the running buffer [20 mM Mops (pH 7.5), 50 mM NaCl, 0.005% P20 surfactant (Biacore) and 5 mM $CaCl_2$] at a flow rate of 20 μl·min^{-1} for 2 min, and the disassociation was monitored for 10 min immediately afterwards. The sensorchip was regenerated with running buffer plus 300 mM EDTA. All binding curves were normalized with a blank flow cell and a control curve of the empty analyte injection. The K_d values were calculated assuming a 1:1 or 1:2 (CaM/BRI1) ratio with the Langmuir model. For the 1:2 ratio calculation, the molecular mass of analyte FLAG–BRI1 was taken as 88 kDa corresponding to the putative dimeric protein. The global fitting procedure of the software BIAevaluation 3.0 was used to calculate the K_d value using data from the six binding curves.

LC (liquid chromatography)-MS/MS (tandem MS) analysis

Denatured *E. coli* soluble proteins were digested with trypsin (Promega) and sequentially enriched for phosphopeptides using TiO_2 (Pierce TiO_2 Phosphopeptide Enrichment and Clean-Up Kit) followed by IMAC (immobilized metal-affinity chromatography) (PHOS-Select Iron Affinity gel, Sigma–Aldrich). The insoluble protein fraction (referred to as 'P-bodies' in Supplementary Table S1 at http://www.BiochemJ.org/bj/443/bj4430515add.htm) was treated similarly. LC–MS/MS analysis was performed on a Waters Q-Tof API-US quadrupole–time-of-flight mass spectrometer with a nanoAcquity UPLC (ultra-performance liquid chromatography) system, with a linear gradient of 1–60% acetonitrile in 0.1% formic acid over 60 min. MS/MS data were collected using the Data Directed Analysis method in MassLynx to fragment the top four ions in each survey scan. Spectra were searched in MAS-COT (http://www.matrixscience.com/search_form_select.html) against the NCBI non-redundant database limited to *E. coli*.

Fluorescence spectroscopy

Fluorescence spectra were acquired at room temperature (21±1°C) with a PTI QuantaMaster4 spectrofluorimeter (Photon Technology) using excitation and emission bandwidths of 5 nm. The tryptophan residues of BRI1 W980 peptide were excited at 285 nm, and fluorescence emission was measured from 300 to 450 nm. Peptide concentrations were either 1 or 2 μM. Measurements were made in buffer consisting of 20 mM Hepes/KOH (pH 7.2), 100 mM KCl and 1 mM $CaCl_2$ or 5 mM EDTA. Purified recombinant CaM was prepared as described previously [27] and added as described in the Figure legends. For each concentration of CaM tested, the fluorescence of a blank consisting of identical reagents minus peptide was recorded and subtracted from the corresponding fluorescence spectrum containing peptide using the instrument software to account for the small contribution of fluorescence from the phenylalanine and tyrosine residues of CaM. Spectra were exported from the instrument software to Origin v8.0 for graphic presentation.

Dansylated CaM was prepared as described in [28]. Fluorescence of the modified protein was excited at 335 nm and emission was recorded from 400 to 600 nm. Fluorescence was measured in 20 mM Hepes/KOH (pH 7.2) and 100 mM KCl containing 150 nM dansylated CaM and recorded after sequential additions of 1 mM $CaCl_2$, 300 nM peptide and 5 mM EDTA. Peptides representing the CaM-binding domains of CaMKII (Ca^{2+}/CaM-dependent protein kinase II) and *Arabidopsis* CNGC2 (cyclic nucleotide-gated channel 2) were purchased from EMD Chemicals and GenScript respectively.

Co-expression of CaM and BRI1 in *E. coli*

E. coli cells co-expressing CaM and recombinant FLAG–BRI1 proteins were prepared by transformation of plasmids designed to express CaM proteins into *E. coli* BL21(DE3) pLysS cells (Novagen) harbouring a FLAG–BRI1 expression plasmid. The recombinant BRI1 cytoplasmic domain was expressed from a high-copy-number plasmid under the control of an inducible *tac* promoter. AtCaM proteins were constitutively expressed from a modified version of pACYC184, a low-copy-number plasmid, containing a p15A origin which allows it to coexist in cells with plasmids of the ColE1 compatibility group such as pBR322 [29]. Constitutive CaM expression driven by this plasmid in *E. coli* was confirmed by extracting soluble proteins and CaM proteins as described previously [27] (Supplementary Figure S1 at http://www.BiochemJ.org/bj/443/bj4430515add.htm). CaM proteins were expressed by this construct in *E. coli* at approximately 1 μg/mg of soluble protein, which is comparable with CaM concentrations in extracts from plants [30].

Recombinant protein purification and immunoblot analysis

Purification of FLAG–BRI1 protein was performed as described in [11] using anti-FLAG M2 affinity gel. Autophosphorylation of the recombinant BRI1 proteins purified from co-expressing *E. coli* cells was analysed by immunoblotting after transfer on to PVDF membranes using Pro-Q Diamond phosphoprotein stain (Invitrogen), anti-phosphotyrosine or anti-phosphothreonine antibodies with the detection of immune complexes using fluorescent secondary antibodies (Invitrogen) as described in [11]. Immunoblotting was carried out as described in [31], and densitometry was performed using an Odyssey Infrared Imaging System (LI-COR Bioscience) to quantify immunoblot results. Relative autophosphorylation levels of BRI1 co-expressed with CaM were calculated as the ratio of the specific phosphorylation signal to the anti-FLAG or Coomassie Brilliant Blue-stained protein signal and the values obtained with the control FLAG–BRI1 cytoplasmic domain expressed alone in *E. coli* were set as 1.

RESULTS AND DISCUSSION

Ca^{2+}-dependent binding of CaM to the BRI1 kinase domain

The interaction of CaM with the BRI1 cytoplasmic domain and its Ca^{2+}-dependence were tested by pull-down assays (Figure 1). When His$_6$–AtCaM7 was immobilized on Ni-NTA–agarose beads, recombinant FLAG–BRI1 protein bound to the beads in the presence of Ca^{2+} (Figure 1A). No binding was observed in the absence of Ca^{2+} or to the Ni-NTA–agarose beads in the absence of bound AtCaM7 (bead control, Figure 1A). Interestingly, CaM binding occurred primarily to the hypophosphorylated form of BRI1 (Figure 1A). In the supernatant fraction, the characteristic upper and lower bands of the FLAG–BRI1 protein (corresponding to hyper- and hypo-phosphorylated forms respectively) were clearly apparent as visualized by an approximate 1:2.9 ratio in densitometry, but primarily the lower band was retained on the AtCaM7-affinity resin (1:15 ratio in densitometry between hyper- and hypo-phosphorylated forms). These results suggest that phosphorylation, perhaps of specific sites, of BRI1 inhibits CaM binding. In order to determine which portion of the BRI1 cytoplasmic domain contained the CaM-binding site, a pull-down experiment was performed with truncated BRI1 proteins lacking either or both of the domains flanking the kinase domain. As shown in Figure 1(B), all of the truncated proteins bound to
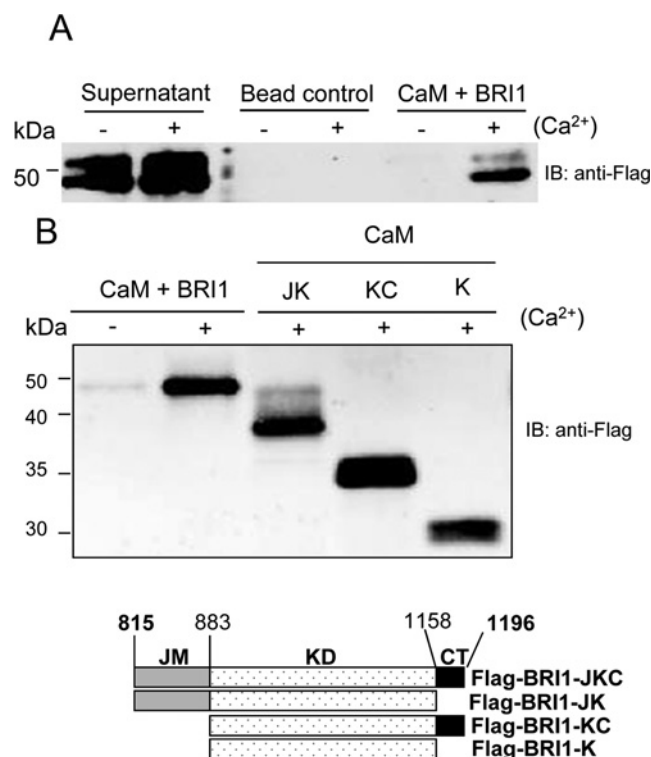

Figure 1   Interaction of CaM with BRI1

(**A**) Binding of FLAG–BRI1 to AtCaM7–Ni-NTA–agarose beads in the presence (+) or absence (−) of Ca^{2+}. The 'bead control' refers to FLAG–BRI1 applied to Ni-NTA beads alone, and 'CaM + BRI1' refers to FLAG–BRI1 applied to AtCaM7–Ni-NTA–agarose beads. Proteins retained by the beads were eluted with sample buffer and analysed by SDS/PAGE followed by immunoblotting (IB) with anti-FLAG antibodies. (**B**) Schematic map of the truncated BRI1-CD domains (KD, KDCT, JMKD and CD) and their binding to AtCaM7–Ni-NTA–agarose beads in the presence (+) or absence (−) of Ca^{2+} as judged by SDS/PAGE and immunoblotting (IB) using anti-FLAG. JM, juxtamembrane region; KD, kinase domain; CT, C-terminal region. Molecular masses are indicated in kDa.

immobilized AtCaM7, suggesting that the CaM-binding site was located within the kinase domain of BRI1.

We confirmed the binding of BRI1 and CaM using real-time measurements of protein–protein interaction. As shown in Figure 2, immobilized His$_6$–CaM7 bound FLAG–BRI1 cytoplasmic domain protein in the presence of Ca^{2+}. The calculated K_d value was ∼58 nM, which is similar to the binding constant for other CaM-interacting proteins, and, when calculated at a 1:2 (CaM/BRI1) binding ratio (see Figure 5), the K_d value was reduced to 13 nM.

CaM binds to BRI1 kinase subdomain VIa

Using algorithms for predicting CaM-binding domains [32], we identified a potential CaM-binding region in the BRI1 kinase domain (Supplementary Figure S2 at http://www.BiochemJ.org/bj/443/bj4430515add.htm). The sequence contains a tryptophan residue, which is often, but not always, found in CaM-binding sites, and structural modelling of the BRI1 kinase domain suggested that this region resides in surface-localized α-helix E of BRI1 kinase subdomain VIa (Supplementary Figure S3 at http://www.BiochemJ.org/bj/443/bj4430515add.htm). A basic amphiphilic α-helix structure is one of the common features found in most CaM-binding proteins characterized [33]. To test whether the predicted sequence could bind CaM, a synthetic peptide (designated W980 from Ala^{974} to Phe^{996} of BRI1)
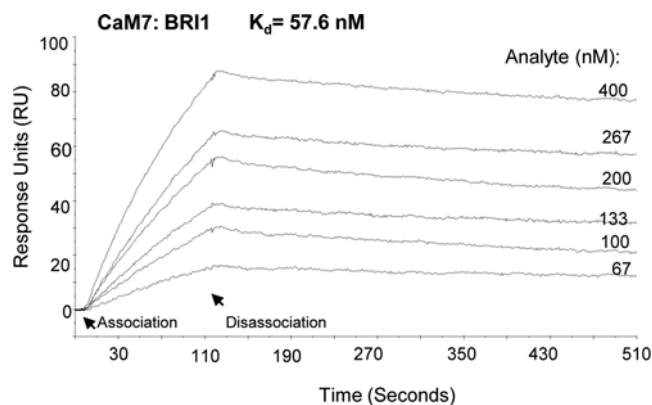
Figure 2   SPR analysis of the CaM–BRI1 interaction

The real-time CaM–BRI1 interaction was analysed by SPR using a Biacore™ 3000 system. The ligand was His_6–AtCaM7 protein that was immobilized ($\sim$300 RU) and the indicated concentrations of FLAG–BRI1 cytoplasmic domain protein were applied as analyte. The disassociation was monitored for 10 min, but only the first 6 min are shown. Binding curves were normalized with a blank flow cell and a control curve of empty analyte injection, and the K_d value was calculated with the Langmuir model in BIAevaluation 3.0 using data from the six binding curves.

Figure 3   CaM interaction with peptides derived from BRI1 and known CaM-binding proteins

(**A**) Binding of His_6–AtCaM7 to immobilized biotin–W980 peptide bound to neutravidin–agarose beads in the presence ($+$) or absence ($-$) of Ca^{2+}. His_6–AtCaM7 proteins that bound were subsequently eluted and subjected to SDS/PAGE and immunoblotting (IB) using anti-His_6 antibodies. A molecular mass of 17 kDa is indicated. (**B**–**E**) Dansylated AtCaM2 (500 nM) in 20 mM Hepes/KOH (pH 7.2) and 100 mM KCl was incubated with a 2-fold molar excess of peptides derived from (**B**) BRI1 W1099, (**C**) BRI1 W980, (**D**) CaMKII or (**E**) CNGC2. Dansylated CaM fluorescence was excited at 335 nm and emission was measured from 400 to 600 nm. In each panel, trace 'a' (continuous line) is the spectrum of dansyl-CaM + Ca^{2+}, trace 'b' (dashed line) is dansyl-CaM + Ca^{2+} + peptide, and trace 'c' (dotted line) is the mixture after chelating the Ca^{2+} with EDTA.

spanning the potential CaM-binding domain was immobilized and tested for CaM binding in a pull-down assay (Figure 3A). As predicted, the W980 peptide interacted with His_6–AtCaM7 and the binding was strongly Ca^{2+}-stimulated; densitometry of the retained CaM7 in the presence of Ca^{2+} was 2.7-fold greater than the CaM7 retained in the beads without Ca^{2+}.

As an independent approach, the binding of the W980 peptide to dansylated AtCAM2 was assessed by monitoring fluorescence of the dansyl fluor, which has the advantage that both molecules are free in solution. As shown in Figure 3(C), the W980 peptide increased the dansyl-CaM fluorescence emission and blue-shifted the fluorescence maximum in the presence of Ca^{2+}. Addition of EDTA to the peptide–Ca^{2+}/CaM mixture reduced the fluorescence emission, suggesting that the interaction between CaM and the W980 peptide was Ca^{2+}-dependent. This fluorescence enhancement and Ca^{2+}-sensitivity of dansylated CaM exerted by the W980 peptide was similar to that elicited from peptides derived from previously established CaM-regulated proteins, mammalian CaMKII [34] (Figure 3D) and *Arabidopsis* CNGC2 [35] (Figure 3E). As an additional control, another kinase domain sequence that contains a tryptophan residue (designated W1099 from Leu[1096] to Glu[1115] of BRI1) was produced and tested for binding to dansylated CaM2. As shown in Figure 3(B), there were some shifts in the fluorescence emission spectrum in the complete reaction, indicating some interaction *in vitro*, but, overall, the changes were substantially reduced compared with the W980 peptide or the positive control peptides (Figures 3D and 3E).

As a second independent approach to assess the interaction of the W980 peptide with CaM *in vitro*, we monitored the intrinsic fluorescence of the tryptophan residue in the W980 peptide. This assay can be used because CaM itself does not contain tryptophan residues. Fluorescence emission of the indole ring of tryptophan is a sensitive indicator of its surroundings: when tryptophan is in an aqueous environment, it fluoresces maximally around 355 nm, whereas when it is buried in a hydrophobic region, its fluorescence is enhanced and also blue-shifted [36]. Figure 4(A) shows that when recombinant AtCaM2 was mixed with the W980 peptide in the presence of Ca^{2+}, fluorescence emission was enhanced and its maximum was blue-shifted to 327 nm. Conversely, EDTA
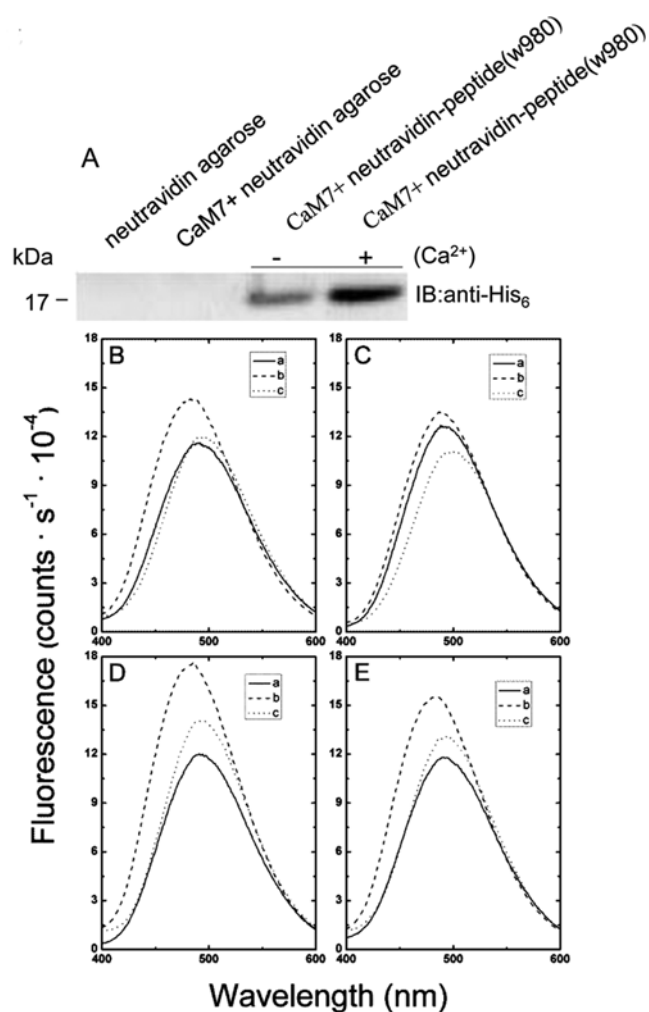
addition reduced fluorescence and red-shifted the maximum to 350 nm. Similar results were obtained with AtCaM4, AtCaM6 and AtCaM7 (Figures 4B–4D). This confirms that binding occurs and suggests further that the indole ring of Trp[980] in the peptide is buried in a hydrophobic pocket of CaM when the two interact. The lack of a shift in the fluorescence emission spectrum of the W980 peptide in the presence of AtCML8 or AtCML9 suggests either that these CML (CaM-like) proteins do not bind to the peptide or that the binding pocket does not position the tryptophan residue in a hydrophobic environment. Nevertheless, two independent in-solution fluorescence-based assays along with demonstration of binding to an immobilized peptide are consistent with the computational prediction of the CaM-binding site as helix E of BRI1 kinase subdomain VIa.
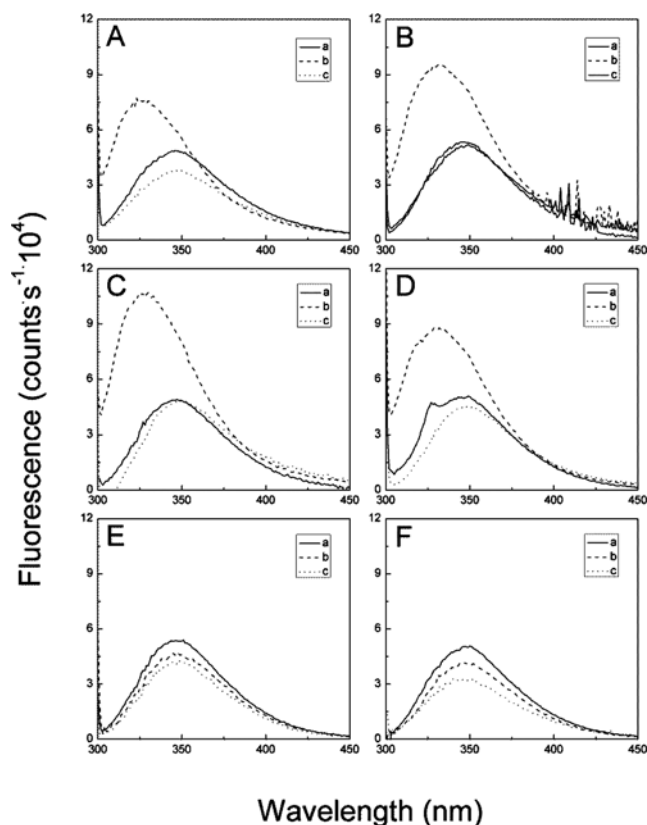
Figure 4   Steady-state tryptophan fluorescence of the BRI1 W980 peptide in the presence of various CaM and CML isoforms

Intrinsic tryptophan fluorescence of the W980 peptide was measured in 20 mM Hepes/KOH (pH 7.2), 100 mM KCl and 1 mM CaCl$_2$ in the presence of (**A**) AtCaM2 (Z12023), (**B**) AtCaM4 (Z12022), (**C**) AtCaM6 (Z12024), (**D**) AtCaM7 (U82119), (**E**) AtCML8 (U84678) or (**F**) AtCML9 (U12490) (GenBank® accession numbers are given within parentheses). In each experiment, emission of 1 μM W980 peptide was measured in the absence of CaM or CML proteins (continuous lines, a) and after sequential addition of 600 nM protein (dashed lines, b) and 5 mM EDTA (dotted lines, c).

Steady-state fluorescence titrations of AtCaM6 with the W980 peptide in the presence of Ca^{2+} were measured because the AtCaM6–W980 peptide combination gave the most robust changes in fluorescence (Figure 4C). The results of this experiment, shown in Figure 5, suggest that the stoichiometry of the AtCaM6–W980 complex is 2:1. To confirm this result, we carried out gel-shift assays [37] on mixtures of AtCaM6 and W980 peptide. As shown in Supplementary Figure S4 (http://www. BiochemJ.org/bj/443/bj4430515add.htm), the mobility of At-CaM6 in a non-denaturing gel containing Ca^{2+} was reduced in the presence of the W980 peptide; the mobility shift saturated at 2 mol equivalents of W980 peptide per mol of AtCaM6. In contrast, the mobility of AtCaM6 was quantitatively shifted in the presence of 1 mol equivalent of a peptide derived from the CaM-binding domain of mammalian CaMKII, a result that is consistent with the known atomic level structure of the CaM–CaMKII complex [34]. The contrast in sharpness between the AtCaM6 complexes with W980 and CaMKII peptides probably reflects their differences in affinity for AtCaM6. Nevertheless, the result is consistent with the idea that the AtCaM6–W980 binding stoichiometry is 2:1. Although somewhat atypical, there are other examples where CaM binds to two polypeptides rather than just one [38]. This could indicate that Ca^{2+}/CaM-mediated signalling may function in some capacity to regulate BRI1 dimerization, but further experiments will be required to test this notion.
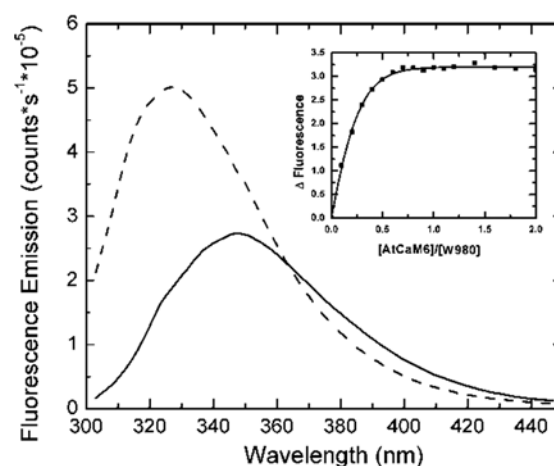

Figure 5   Stoichiometry of binding of AtCaM6 to the W980 peptide using steady-state tryptophan fluorescence

Intrinsic tryptophan fluorescence of W980 (2 μM) was measured in 20 mM Hepes/KOH (pH 7.2), 100 mM KCl and 1 mM CaCl$_2$ following sequential additions of CaM6. Only the curves for 0 (continuous line) and 1 (broken line) mol equivalent of CaM6 are shown for clarity. The inset shows the change in fluorescence intensity (ΔFluorescence) at λ_{max} of the CaM6–W980 complex plotted against the [CaM6]/[W980] ratio. The data were fitted by a Boltzmann function to produce a binding curve using Origin (version 8.0).

AtCaM6 binding does not affect BRI1 kinase activity *in vitro*

We tested the effect of Ca^{2+}/CaM on BRI1 peptide kinase activity using the SP11 synthetic peptide as substrate [10]. As shown in Supplementary Figure S5 (http://www.BiochemJ. org/bj/443/bj4430515add.htm), addition of increasing concentrations of AtCaM6 in the presence or absence of Ca^{2+} had no significant effect on transphosphorylation of the synthetic peptide. Likewise, previous studies found no effect of CaM binding to BoSRK (*Brassica oleracea* S locus receptor kinase) [25] or AtCaMRLK (At CaM-binding RLK) [24].

Co-expression of CaM and BRI1 in *E. coli* inhibits autophosphorylation of BRI1

Another assay of BRI1 kinase activity is autophosphorylation; however, analysis of autophosphorylation in short reactions *in vitro* [10] does not completely reflect the process that occurs *in planta* or when recombinant protein is expressed in *E. coli* [11]. Accordingly, to assess whether autophosphorylation of BRI1 is affected by CaM, we co-expressed the two proteins in *E. coli* and then examined BRI1 autophosphorylation by immunoblotting. As a control, we co-expressed 14-3-3ω, which also binds to the BRI1 cytoplasmic domain (M.-H. Oh, X. Wu and S. C. Huber, unpublished work). As shown in Figure 6, co-expression of CaM with BRI1 altered the pattern of BRI1 autophosphorylation, and, in general, tyrosine autophosphorylation (pTyr in the Figure) of BRI1 was inhibited more strongly than threonine autophosphorylation or overall autophosphorylation as assessed by Pro-Q Diamond phosphoprotein staining. All CaM isoforms tested had some effect, but CaM6, CaM7 and CML8 were more effective than were CaM2, CaM4, CML11 (GenBank® accession number U14842) and 14-3-3ω. The inhibition of BRI1 autophosphorylation is evident from the immunoblot and stain results shown in Figure 6(A), and as quantified in Figure 6(B), where values were normalized for BRI1 protein (Coomassie Brilliant Blue staining). Importantly, the expression of the different CaM isoforms did not vary appreciably as shown in the bottom panel of Figure 6(A), indicating that differences in isoform
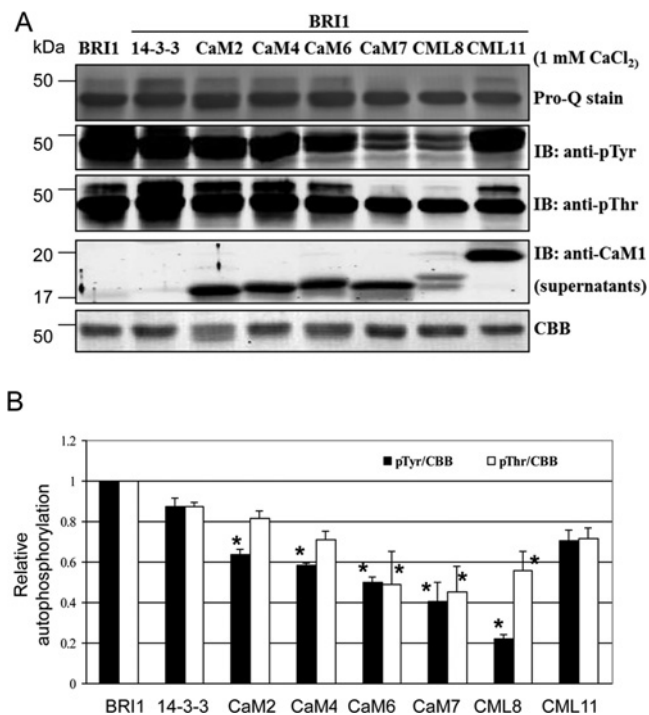
Figure 6   Inhibition of BRI1 autophosphorylation by co-expression of CaM

(**A**) Co-expression of individual CaM or CML isoforms with recombinant BRI1 cytoplasmic domain (CD) in *E. coli* cultured in LB (Luria–Bertani) medium containing 1 mM CaCl$_2$. FLAG–BRI1-CD proteins were separated by SDS/PAGE and analysed for total phosphorylation by Pro-Q staining or for more specific phosphorylation on tyrosine or threonine residues by immunoblotting (IB) using generic antibodies as indicated. Results are representative of four independent experiments. Molecular masses are indicated in kDa. (**B**) The results obtained from immunoblotting were quantified as the relative autophosphorylation levels on tyrosine (black bars) or threonine (white bars), normalized for Coomassie Brilliant Blue (CBB)-stained protein, and values for the BRI1 control were set at 1. *$P \leqslant$ 0.05 relative to the BRI1 control using Student's *t* test.

effectiveness cannot be ascribed to variation in expression level. It is also worth noting that the production of recombinant BRI1 protein was not appreciably altered by co-expression of the second protein (results not shown). These results suggest that interaction with certain CaM isoforms inhibits BRI1 autophosphorylation and that phosphorylation of tyrosine residues may be affected more than serine and threonine residues.

Co-expression of CaM and BRI1 in *E. coli* inhibits transphosphorylation of bacterial proteins

During the production of recombinant BRI1 protein in *E. coli*, bacterial proteins are phosphorylated, which provides a novel assay for the transphosphorylation activity of the BRI1 cytoplasmic domain. The assay has been characterized (details are available from S.C.H. on request), but, in the present paper, we document the basic occurrence of this activity only. After 16 h of BRI1 induction, numerous *E. coli* proteins were phosphorylated as was evident by immunoblotting and Pro-Q Diamond phosphoprotein staining (Figure 7). The phosphorylation of bacterial proteins was dependent on the kinase activity of BRI1, because when the kinase-inactive BRI1(K911E) mutant was expressed, essentially no phosphorylation of *E. coli* proteins was observed (Supplementary Figure S6 at http://www.BiochemJ. org/bj/443/bj4430515add.htm). The samples analysed in Figure 6 had the majority of the FLAG–BRI1 protein removed by affinity-purification, but some of the BRI1 protein was still apparent

at the position expected for a ∼50 kDa protein (Figure 7). The most important result is that co-expression of the CaM isoforms inhibited the transphosphorylation of *E. coli* proteins. This was most apparent with AtCaM6, AtCaM7 and AtCML8, which almost completely inhibited transphosphorylation on threonine and tyrosine residues. The strong reduction in Pro-Q Diamond staining also suggests that serine phosphorylation was also inhibited. Importantly, co-expression of 14-3-3ω had no apparent effect on the transphosphorylation activity of BRI1, indicating that the effects observed with CaM co-expression were specific. The CaM isoform specificity for inhibition of autophosphorylation (Figure 6) was generally similar to that for transphosphorylation (Figure 7), confirming the notion that CaM binding to BRI1 *in situ* attenuated kinase activity. Interestingly, these results also suggest that the lack of apparent binding of CML8 to the W980 peptide *in vitro* (Figure 4E) probably means that the binding pocket of CML8 does not position the tryptophan residue in a hydrophobic environment and therefore the fluorescence emission spectrum is unaltered.

To firmly establish the BRI1-mediated transphosphorylation of *E. coli* proteins, samples such as those used in the immunoblot analysis presented in Figure 7 were digested with trypsin and phosphopeptides were enriched with TiO$_2$ or IMAC before analysis by LC–MS/MS. The two enrichment protocols are considered to be complementary [39–41]. Combining all of the results obtained in the present study, a total of 77 unique phosphopeptides consisting of 104 individual phosphorylation sites were identified. The sites were distributed among 41 different *E. coli* proteins that included many enzymes involved in gene expression, translation, protein folding and metabolism. One example is illustrated in Figure 8(A), but a complete list of the phosphopeptides identified is provided in Supplementary Table S1. As shown in Figure 8(A), the DNA-binding protein hupA was phosphorylated on seven distinct residues that were observed in six different phosphopeptides. Interestingly, the seven phosphorylation sites were located in either the N-terminal or the C-terminal region of the protein. The results with hupA also illustrate that our analysis identified phosphopeptides that included single, doubly and triply phosphorylated peptides, with a predominance of doubly phosphorylated species (Figure 8B). From analysis of the multiply phosphorylated peptides, the number of residues between phosphorylation sites ranged from zero (i.e. adjacent phosphosites) to nine, with the largest number having four intervening residues (Figure 8C). These results are important because they firmly establish this new assay for BRI1-mediated transphosphorylation and perhaps will give insights into the nature of the sites targeted by BRI1, and, in this regard, the predominance of multiply phosphorylated peptides was certainly unexpected. It is important to note that bacterial cells do have endogenous protein phosphorylation on serine, threonine and tyrosine residues, although at much lower levels than in eukaryotes. In an intensive survey [42], 81 phosphorylation sites on 79 *E. coli* proteins were identified, and two of these endogenous phosphosites were detected in our study: Ser[19] of rpmB and Ser[453] of dnaK. It is possible that these sites were also targets of BRI1, but it is clear that the vast majority of the sites reported in Supplementary Table S1 were phosphorylated by BRI1 rather than endogenous bacterial protein kinases.

Concluding remarks

We have shown that Ca^{2+}/CaM binds to the recombinant BRI1 cytoplasmic domain protein *in vitro* and have identified a likely binding site in subdomain VIa. Interestingly, a previous study found that CaM binds to BoSRK [25] at the equivalent site
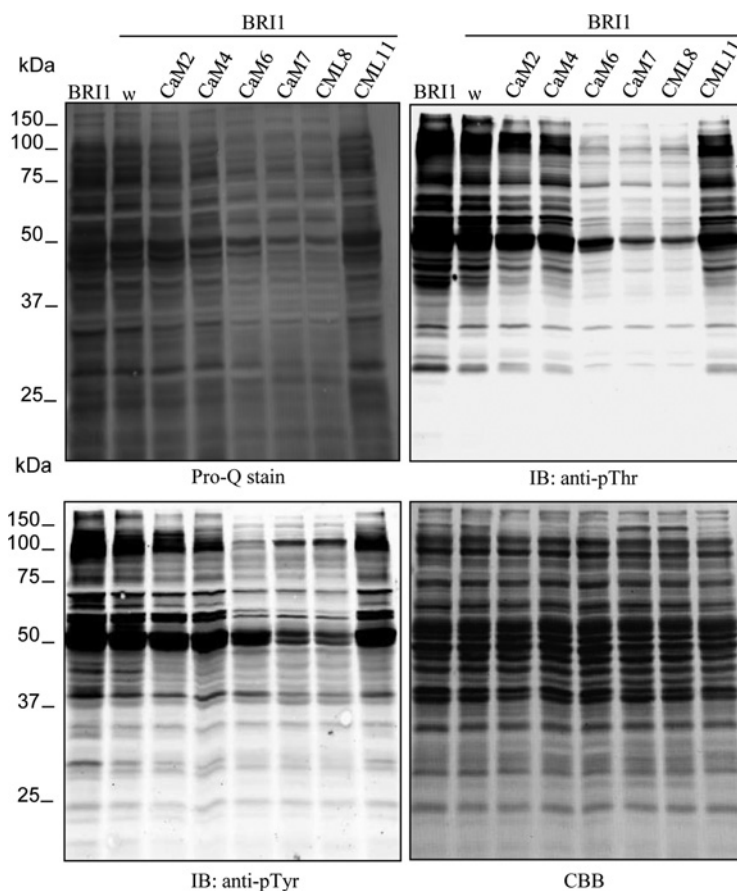
Figure 7   Inhibition of BRI1-mediated transphosphorylation of *E. coli* proteins by co-expression of CaM proteins

Following affinity-purification of FLAG–BRI1 protein from cultures co-expressing CaM or CML isoforms, aliquots (containing 15 μg of predominantly *E. coli* proteins) of the remaining protein fraction were separated by SDS/PAGE and analysed for phosphorylation as described in Figure 6. w, 14-3-3ω; CBB, Coomassie Brilliant Blue; IB, immunoblotting. Molecular masses are indicated in kDa.

in subdomain VIa and because of general conservation of this region, these authors suggested that CaM may interact with other receptor kinases. Indeed, binding of CaM to RLK4 and CLV1 (CLAVATA1) was demonstrated, but BRI1 was reported to not bind [25]; the basis for the discrepancy in results with BRI1 is not clear. However, what is emerging is that CaM appears to interact broadly with plant receptor kinases, including BoSRK, AtRLK4 and AtCLV1 [25], AtCaMRLK [24] and, in the present study, BRI1. Previous studies reported that CaM had no effect on the activity of these kinases, and thus our demonstration that CaM inhibits BRI1 kinase activity when co-expressed in *E. coli* provides the first information about a possible functional impact of CaM binding. The inhibition of BRI1 autophosphorylation and transphosphorylation activity by co-expression of certain CaM isoforms provides compelling evidence for the notion that CaM binding affects BRI1 kinase activity. Moreover, the results uncover a possible link between Ca^{2+} and BR signalling that will provide the foundation for future studies.

In the present study, we also established a new assay for monitoring transphosphorylation activity of recombinant receptor kinase cytoplasmic domains. This assay is based on the phosphorylation of *E. coli* proteins *in situ* as a result of expression of the recombinant protein kinase and is documented in the present study for BRI1. The assay will almost certainly will have relevance to studies with other receptor kinases as well. In the present study, we have established by immunoblotting

that BRI1 phosphorylates numerous *E. coli* proteins on serine, threonine and tyrosine residues (Figure 7). Many specific serine and threonine phosphosites on *E. coli* proteins were identified by LC–MS/MS (Figure 8 and Supplementary Table S1). It is not clear why we were unable to identify any tyrosine phosphosites, but this perhaps reflects their lower relative abundance compared with serine/threonine phosphosites. Of particular relevance to the present study, we used the new assay to demonstrate the inhibitory effect of CaM on BRI1-mediated transphosphorylation activity (Figure 7). Isoforms of CaM and CML proteins differed in their effectiveness and those that inhibited transphosphorylation also inhibited BRI1 autophosphorylation. We observed that AtCaM6 and AtCaM7 were more effective than were AtCaM2 and AtCaM4, and, indeed, CaM6 and CaM7 are most similar to one another in sequence [43]. Interestingly, CML8 was as effective as CaM6 and CaM7 (Figures 6 and 7), suggesting that non-canonical CaM-like proteins may play a role in BRI1 regulation as well. Although the CML family has 50 members, CML8 and its paralogue CML11 are most closely related to the CaM proteins, but differed strikingly in their ability to affect BRI1 kinase activity, with CML11 being inactive. Thus subtle sequence differences can have dramatic effects, as has been observed previously for interactions of CaM isoforms with their target proteins [44,45].

The results of the present study raise many important questions that remain to be addressed. First, do BRI1 and CaM/CML proteins interact *in vivo*, and, if so, under what conditions?

A Phosphorylation sites on *E. coli* hupA

| Source	Site	M_r(expt)	M_r(calc)	Delta	MC	Score	Expect	Peptide
TiO	T4	1581.3848	1581.7837	-0.3989	1	101	1.40E-08	-.MNK**pT**QLIDVIAEK.A
IMAC	T19	1054.2634	1054.506	-0.2425	1	30	0.018	K.AELSK**pT**QAK.A
IMAC	S17T19	1134.2084	1134.4723	-0.2638	1	45	0.00029	K.AEL**pS**K**pT**QAK.A
TiO	S27T33	1676.3594	1676.7674	-0.4080	0	53	2.40E-05	K.AALE**pS**TLAAI**pT**ESLK.E
TiO	T28T33	1676.3608	1676.7674	-0.4066	0	57	8.90E-06	K.AALES**pT**LAAI**pT**ESLK.E
TiO	S81	1323.3224	1323.6588	-0.3363	0	79	2.00E-07	K.IAAANVPAFV**pS**GK.A
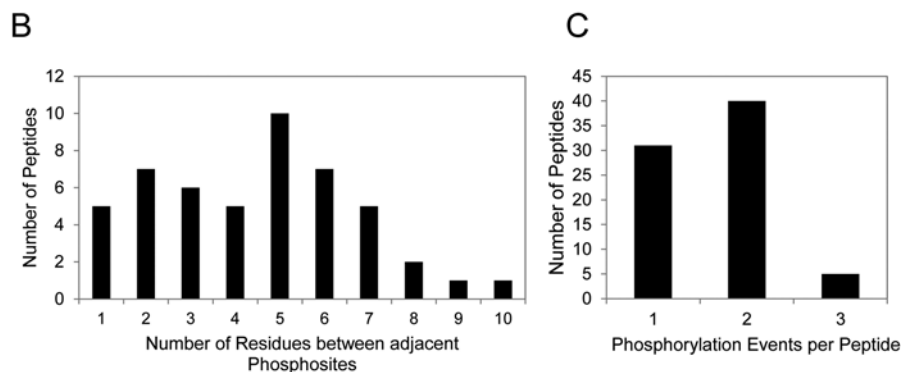
Figure 8   Identification of BRI1-mediated transphosphorylation sites on *E. coli* proteins

(**A**) Representative LC–MS/MS results identifying BRI1-mediated phosphorylation sites on the DNA-binding protein hupA, obtained by enrichment of phosphopeptides using TiO_2 (TiO) or Fe^{3+}-IMAC (IMAC) as indicated. The complete list of phosphosites identified is presented in Supplementary Table S1 at http://www.BiochemJ.org/bj/443/bj4430515add.htm. M_r(expt), expected molecular mass; M_r(calc), calculated molecular mass; MC, the number of missed cleavages; Score, Mascot score, which is a probability-based implementation of the Mowse algorithm. The total score is the absolute probability that the observed match is a random event and is calculated as $-10 \cdot \log_{10}(P)$, where P is the absolute probability. Expect, expectation value, which is directly equivalent to the E-value in a BLAST search result. The lower the expectation value, the more significant the score. (**B**) Number of residues between adjacent phosphosites in multiply phosphorylated peptides. (**C**) Number of singly, doubly or triply phosphorylated peptides identified.

Presumably the interaction is regulated by increased cytosolic Ca^{2+} concentrations, which could occur under stress conditions [46,47] or in response to BR signalling [48]. Another important question is whether the inhibition of transphosphorylation activity by Ca^{2+}/CaM binding to BRI1 occurs as a result of the inhibition of autophosphorylation. This is our current working model (Supplementary Figure S7), which we believe explains why addition of CaM *in vitro* had no effect on BRI1 peptide kinase activity (Supplementary Figure S5). If correct, then a rise in cytosolic Ca^{2+} concentration that occurs after the receptor kinase has fully activated would have no immediate consequence on kinase activity, but rather would inhibit the subsequent activation of additional BRI1 molecules. Another crucial area for future research will be to identify all of the downstream cytoplasmic targets (e.g. other protein kinases) that are transphosphorylated directly by BRI1 *in vivo* in *Arabidopsis* cells, the influence of phosphorylation on their biological functions, and roles that Ca^{2+} and CaM or CML proteins may have in this process, particularly in plants acclimating to biotic or abiotic stress. Although many questions remain, the new insights obtained provide a working model and foundation for continued studies. Moreover, the co-expression system in *E. coli* may be useful for studies of CaM and other proteins as potential interactors with a variety of receptor kinases.

AUTHOR CONTRIBUTION

Man-Ho Oh, Hyoung Kim, Xia Wu and Ray Zielinski conducted experiments, contributed to data analysis and preparation of the paper. Steven Clouse contributed to data discussion and preparation of the paper. Ray Zielinski and Steven Huber designed experiments, contributed to data analysis and discussion and assembled the paper.

REFERENCES

1   Chae, L., Sudat, S., Dudoit, S., Zhu, T. and Luan, S. (2009) Diverse transcriptional programs associated with environmental stress and hormones in the *Arabidopsis* receptor-like kinase gene family. Mol. Plant **2**, 84–107

2   Lehti-Shiu, M. D., Zou, C., Hanada, K. and Shiu, S.-H. (2009) Evolutionary history and stress regulation of plant receptor-like kinase/Pelle genes. Plant Physiol. **150**, 12–26

3   Nurnberger, T. and Kemmerling, B. (2006) Receptor protein kinases: pattern recognition receptors in plant immunity. Trends Plant Sci. **11**, 519–522

4   Clouse, S. D. (2011) Brassinosteroid signal transduction: from receptor kinase activation to transcriptional networks regulating plant development. Plant Cell **23**, 1219–1230

5   Li, J. and Chory, J. (1997) A putative leucine-rich repeat receptor kinase involved in brassinosteroid signal transduction. Cell **90**, 929–938

6   Nam, K. H. and Li, J. (2002) BRI1/BAK1, a receptor kinase pair mediating brassinosteroid signaling. Cell **110**, 203–212

7   Shiu, S. H. and Bleecker, A. B. (2001) Receptor-like kinases from *Arabidopsis* form a monophyletic gene family related to animal receptor kinases. Proc. Natl. Acad. Sci. U.S.A. **98**, 10763–10768

8   Kinoshita, T., Cano-Delgado, A., Seto, H., Hiranuma, S., Fujioka, S., Yoshida, S. and Chory, J. (2005) Binding of brassinosteroids to the extracellular domain of plant receptor kinase BRI1. Nature **433**, 167–171

9   Wang, Z. Y., Seto, H., Fujioka, S., Yoshida, S. and Chory, J. (2001) BRI1 is a critical component of a plasma-membrane receptor for plant steroids. Nature **410**, 380–383

10   Oh, M.-H., Ray, W. K., Huber, S. C., Asara, J. M., Gage, D. A. and Clouse, S. D. (2000) Recombinant brassinosteroid insensitive 1 receptor-like kinase autophosphorylates on serine and threonine residues and phosphorylates a conserved peptide motif *in vitro*. Plant Physiol. **124**, 751–766

11   Oh, M.-H., Wang, X., Kota, U., Goshe, M. B., Clouse, S. D. and Huber, S. C. (2009) Tyrosine phosphorylation of the BRI1 receptor kinase emerges as a component of brassinosteroid signaling in *Arabidopsis*. Proc. Natl. Acad. Sci. U.S.A. **106**, 658–663

12   Friedrichsen, D. M., Joazeiro, C. A., Li, J., Hunter, T. and Chory, J. (2000) Brassinosteroid-insensitive-1 is a ubiquitously expressed leucine-rich repeat receptor serine/threonine kinase. Plant Physiol. **123**, 1247–1256

13   Wang, X., Goshe, M. B., Soderblom, E. J., Phinney, B. S., Kuchar, J. A., Li, J., Asami, T., Yoshida, S., Huber, S. C. and Clouse, S. D. (2005) Identification and functional analysis of *in vivo* phosphorylation sites of the *Arabidopsis* BRASSINOSTEROID-INSENSITIVE1 receptor kinase. Plant Cell **17**, 1685–1703

14   Wang, X., Kota, U., He, K., Blackburn, K., Li, J., Goshe, M. B., Huber, S. C. and Clouse, S. D. (2008) Sequential transphosphorylation of the BRI1/BAK1 receptor kinase complex impacts early events in brassinosteroid signaling. Dev. Cell **15**, 220–235

15   He, J.-X., Gendron, J. M., Sun, Y., Gampala, S. S. L., Gendron, N., Sun, C. Q. and Wang, Z.-Y. (2005) BZR1 is a transcriptional repressor with dual roles in brassinosteroid homeostasis and growth responses. Science **307**, 1634–1638

16   Vert, G., Nemhauser, J. L., Geldner, N., Hong, F. and Chory, J. (2005) Molecular mechanisms of steroid hormone signaling in plants. Annu. Rev. Cell Dev. Biol. **21**, 177–201

17   Oh, M.-H., Wang, X., Wu, X., Zhao, Y., Clouse, S. D. and Huber, S. C. (2010) Autophosphorylation of Tyr-610 in the receptor kinase BAK1 plays a role in brassinosteroid signaling and basal defense gene expression. Proc. Natl. Acad. Sci. U.S.A. **107**, 17827–17832

18   Oh, M.-H., Clouse, S. D. and Huber, S. C. (2009) Tyrosine phosphorylation in brassinosteroid signaling. Plant Signaling Behav. **4**, 1–4

19   Ma, W. and Berkowitz, G. A. (2007) The grateful dead: calcium and cell death in plant innate immunity. Cell. Microbiol. **9**, 2571–2585

20   McAinsh, M. R. and Pittman, J. K. (2009) Shaping the calcium signature. New Phytol. **181**, 275–294

21   Bouche, N., Yellin, A., Snedden, W. A. and Fromm, H. (2005) Plant-specific calmodulin-binding proteins. Annu. Rev. Plant Biol. **56**, 435–466

22   DeFalco, T. A., Bender, K. W. and Snedden, W. A. (2009) Breaking the code: Ca^{2+} sensors in plant signalling. Biochem. J. **425**, 27–40

23   Du, L. and Poovaiah, B. W. (2005) Ca^{2+}/calmodulin is critical for brassinosteroid biosynthesis and plant growth. Nature **437**, 741–745

24   Charpenteau, M., Jaworski, K., Ramirez, B. C., Tretyn, A., Ranjeva, R. and Ranty, B. (2004) A receptor-like kinase from *Arabidopsis thaliana* is a calmodulin-binding protein. Biochem. J. **379**, 841–848

25   Vanoosthuyse, V., Tichtinsky, G., Dumas, C., Gaude, T. and Cock, J. M. (2003) Interaction of calmodulin, a sorting nexin and kinase-associated protein phosphatase with the *Brassica oleracea* S locus receptor kinase. Plant Physiol. **133**, 919–929

26   Humphrey, W., Dalke, A. and Schulten, K. (1996) VMD: visual molecular dynamics. J. Mol. Graphics **14**, 27–38

27   Zielinski, R. E. (2002) Preparation of recombinant plant calmodulin isoforms. Methods Mol. Biol. **172**, 143–149

28   Kincaid, R. L., Billingsley, M. L. and Vaughan, M. (1988) Preparation of fluorescent, cross-linking, and biotinylated calmodulin derivatives and their use in studies of calmodulin-activated phosphodiesterase and protein phosphatase. Methods Enzymol. **159**, 605–626

29   Chang, A. C. and Cohen, S. N. (1978) Construction and characterization of amplifiable multicopy DNA cloning vehicles derived from the P15A cryptic miniplasmid. J. Bacteriol. **134**, 1141–1156

30   Zielinski, R. E. (1998) Calmodulin and calmodulin-binding proteins in plants. Annu. Rev. Plant Physiol. Plant Mol. Biol. **49**, 697–725

31   Duncan, K. A., Hardin, S. C. and Huber, S. C. (2006) The three maize sucrose synthase isoforms differ in distribution, localization, and phosphorylation. Plant Cell Physiol. **47**, 959–971

32   Yap, K. L., Kim, J., Truong, K., Sherman, M., Yuan, T. and Ikura, M. (2000) Calmodulin target database. J. Struct. Funct. Genomics **1**, 8–14

33   Rainaldi, M., Yamniuk, A. P., Murase, T. and Vogel, H. J. (2007) Calcium-dependent and -independent binding of soybean calmodulin isoforms to the calmodulin binding domain of tobacco MAPK phosphatase-1. J. Biol. Chem. **282**, 6031–6042

34   Meador, W. E., Means, A. R. and Quiocho, F. A. (1993) Modulation of calmodulin plasticity in molecular recognition on the basis of X-ray structures. Science **262**, 1718–1721

35   Hua, B.-G., Mercier, R. W., Zielinski, R. E. and Berkowitz, G. A. (2003) Functional interaction of calmodulin with a plant cyclic nucleotide gated cation channel. Plant Physiol. Biochem. **41**, 945–954

36   Burstein, E. A., Vedenkina, N. S. and Ivkova, M. N. (1973) Fluorescence and the location of tryptophan residues in protein molecules. Photochem. Photobiol. **18**, 263–279

37   Erickson-Viitanen, S. and DeGrado, W. F. (1987) Recognition and characterization of calmodulin-binding sequences in peptides and proteins. Methods Enzymol. **139**, 455–478

38   Giedroc, D. P., Ling, N. and Puett, D. (1983) Identification of β-endorphin residues 14–25 as a region involved in the inhibition of calmodulin-stimulated phosphodiesterase activity. Biochemistry **22**, 5584–5591

39   Larsen, M. R., Thingholm, T. E., Jensen, O. N., Roepstorff, P. and Jørgensen, T. J. D. (2005) Highly selective enrichment of phosphorylated peptides from peptide mixtures using titanium dioxide microcolumns. Mol. Cell. Proteomics **4**, 873–886

40   Wilson-Grady, J. T., Villén, J. and Gygi, S. P. (2008) Phosphoproteome analysis of fission yeast. J. Proteome Res. **7**, 1088–1097

41   Carrascal, M., Ovelleiro, D., Casas, V., Gay, M. and Abian, J. (2008) Phosphorylation analysis of primary human T lymphocytes using sequential IMAC and titanium oxide enrichment. J. Proteome Res. **7**, 5167–5176

42   Macek, B., Gnad, F., Soufi, B., Kumar, C., Olsen, J. V., Mijakovic, I. and Mann, M. (2008) Phosphoproteome analysis of *E. coli* reveals evolutionary conservation of bacterial Ser/Thr/Tyr phosphorylation. Mol. Cell. Proteomics **7**, 299–307

43   McCormack, E., Tsai, Y.-C. and Braam, J. (2005) Handling calcium signaling: *Arabidopsis* CaMs and CMLs. Trends Plant Sci. **10**, 383–389

44   Bhattacharya, S., Bunick, C. G. and Chazin, W. J. (2004) Target selectivity in EF-hand calcium binding proteins. Biochim. Biophys. Acta **1742**, 69–79

45   Kohler, C. and Neuhaus, G. (2000) Characterisation of calmodulin binding to cyclic nucleotide-gated ion channels from *Arabidopsis thaliana*. FEBS Lett **471**, 133–136

46   Kader, M. A. and Lindberg, S. (2010) Cytosolic calcium and pH signaling in plants under salinity stress. Plant Signaling Behav. **5**, 233–238

47   Zhu, J.-K. (2002) Salt and drought stress signal transduction in plants. Annu. Rev. Plant Biol. **53**, 247–273

48   Yichen, Z., Qi, Z., Wheeler, J., Kwezi, L., Irving, H., Gehring, C. and Berkowitz, G. A. (2010) Teaching an old hormone new tricks: BR receptor-mediated Ca^{2+} signaling. In Plant Biology 2010, Montreal, Canada, 31 July–4 August 2010, Abstract M1302 (http://abstracts.aspb.org/pb2010/public/M13/M1302.html)

Calcium/calmodulin inhibition of the *Arabidopsis* BRASSINOSTEROID-INSENSITIVE 1 receptor kinase provides a possible link between calcium and brassinosteroid signalling

Man-Ho OH*, Hyoung Seok KIM*, Xia WU*, Steven D. CLOUSE†, Raymond E. ZIELINSKI* and Steven C. HUBER*‡[1]

*Department of Plant Biology, University of Illinois, Urbana, IL 61801, U.S.A., †Department of Horticultural Science, NC State University, Raleigh, NC 27695, U.S.A., and ‡U.S. Department of Agriculture, Agricultural Research Service, Urbana, IL 61801, U.S.A.
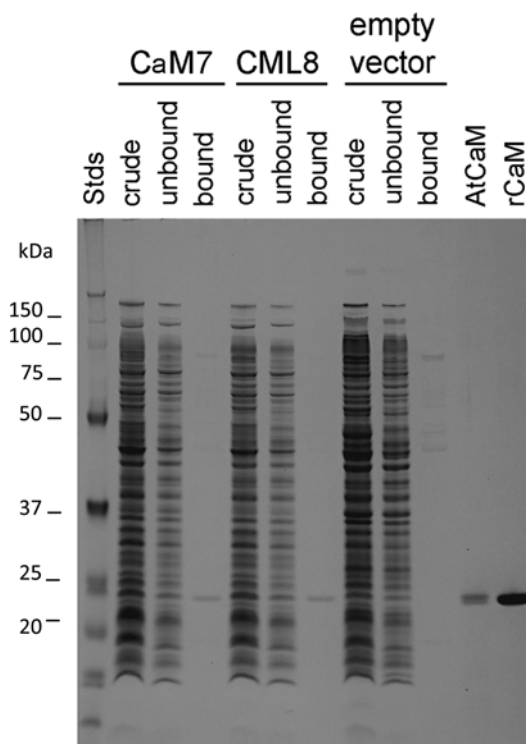
Figure S1   Constitutive expression of CaM in *E. coli* driven by pRZ528 (CaM7) and 529 (CML8)

Total soluble proteins were extracted from late-exponential-phase bacteria, clarified by centrifugation and subjected to Ca^{2+}-dependent HIC (hydrophobic interaction chromatography) on phenyl-Sepharose. Samples of the crude extract, the fraction that did not bind to phenyl-Sepharose (unbound), and the fraction that eluted from the resin in the presence of EDTA (bound) were separated by SDS/PAGE and stained with Coomassie Brilliant Blue. Purified AtCaM and recombinant CaM (rCaM) were fractionated in parallel as positive controls together with molecular mass standards (Stds, sizes given in kDa).

Figure S2   BRI1 cytoplasmic domain sequence showing predicted probabilities of CaM binding

The numbers below the sequence indicate the probability of CaM binding (http://calcium.uhnres.utoronto.ca/ctdb/ctdb/home.html) with 9 being the highest score. The kinase domain of BRI1 is shown in red, and the sequences used to generate the W980 and W1099 peptides are underlined.

---

[1]   To whom correspondence should be addressed (email schuber1@illinois.edu).

A Front view   B Side view
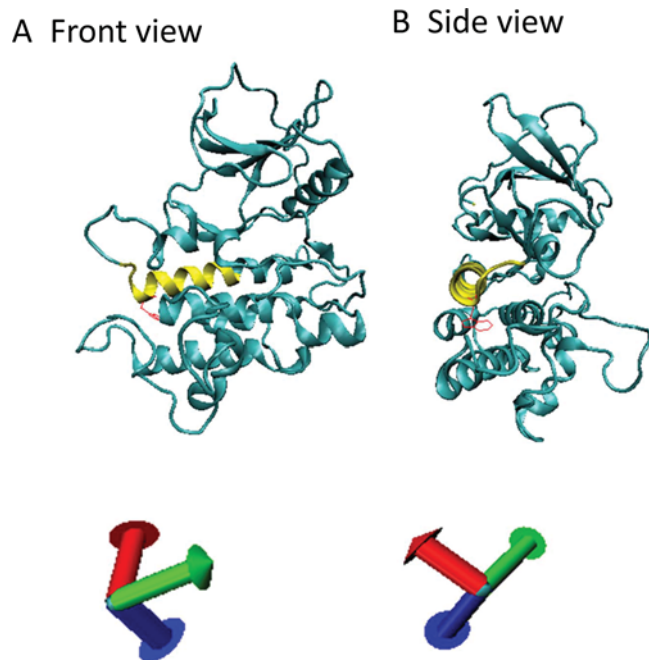
Figure S3   Model of the BRI1 kinase domain structure

The BRI1 kinase domain was modelled as described in the Experimental section of the main text. The location of the predicted CaM-binding site (Leu[978]–Arg[992]) is shown in yellow and the Try[980] side chain is shown in red. (**A**) Front view. (**B**) Side view.
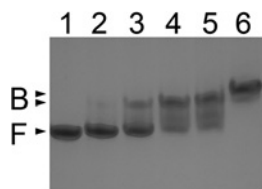
Figure S4   Gel mobility-shift analysis of AtCaM6 interaction with W980 peptide

AtCaM6 (300 pmol/reaction) was incubated with 0 (lane 1), 150 (lane 2), 300 (lane 3), 600 (lane 4) or 1200 (lane 5) pmol of W980 peptide or 300 pmol of a CaM-binding peptide from CaMKII (lane 6) then fractionated in a non-denaturing gel containing Ca^{2+}. Coomassie Brilliant Blue staining revealed the migration of free (F) and peptide-bound (B) AtCaM6. The larger size of the CaMKII peptide resulted in a slower mobility of the peptide–AtCaM6 complex compared with the W980 peptide complex.
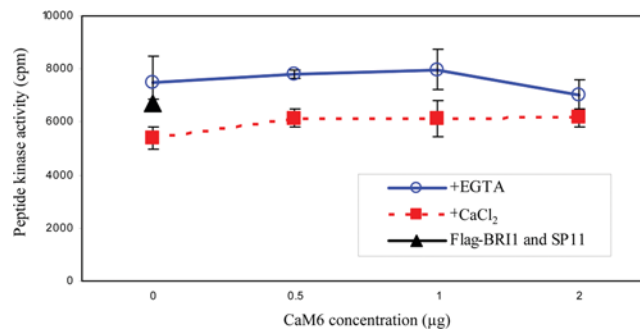
Figure S5   AtCaM6 has no effect on BRI1 peptide kinase activity *in vitro*

BRI1 peptide kinase activity was assayed using [^{32}P]ATP and the SP11 synthetic peptide as substrate as described in [1] with the addition of 0.1 mM $CaCl_2$ or 1 mM EGTA as indicated. Each reaction contained 0.5 μg of FLAG–BRI1 protein, and reactions were run for 5 min.
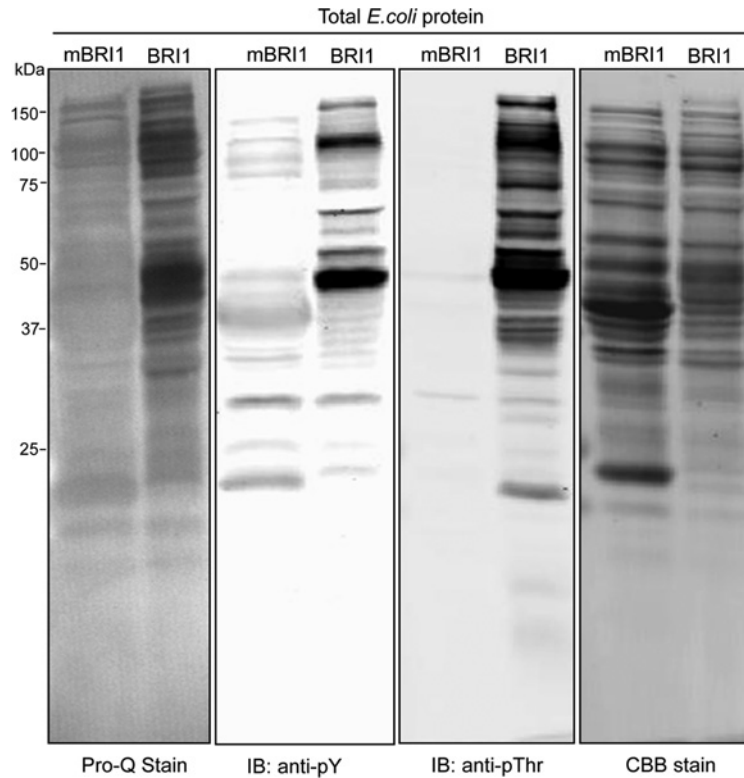
Figure S6   Kinase-inactive mBRI1 does not transphosphorylate *E. coli* proteins

BRI1 or the kinase-inactive mBRI1 (mutant BRI1) were expressed in *E. coli* and following purification of the FLAG-tagged proteins, the remaining *E. coli* proteins were analysed for phosphorylation by Pro-Q Diamond phosphoprotein staining or immunoblotting (IB) with generic anti-phosphotyrosine or anti-phosphothreonine antibodies. Molecular masses are indicated in kDa.
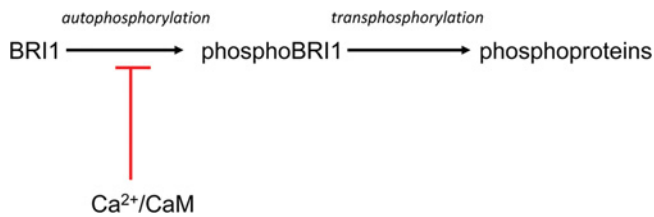
Figure S7   Working model for effects of Ca^{2+}/CaM on BRI1

We propose that Ca^{2+}/CaM inhibits BRI1 autophosphorylation, which then affects transphosphorylation activity. Thus certain CaM and CML isoforms inhibit BRI1 autophosphorylation when co-expressed in *E. coli* and, as a result, also inhibit the transphosphorylation of *E. coli* proteins. This provides a plausible explanation for why Ca^{2+}/CaM inhibits transphosphorylation in the *in situ* system, but does not affect transphosphorylation activity *in vitro* (peptide kinase activity). The model predicts that Ca^{2+} signalling during early stages of BRI1 activation will attenuate downstream signal transduction.

Table S1   Identification of BRI1-mediated phosphorylation sites on *E. coli* proteins

LC–MS/MS results identifying BRI1-mediated phosphorylation sites on *E. coli* proteins, obtained by enrichment of phosphopeptides using TiO_2, Fe^{3+}-IMAC (IMAC) or processing bodies (P-bodies) as indicated. M_r(expt), expected molecular mass; M_r(calc), calculated molecular mass; MC, the number of missed cleavages; Score, Mascot score, which is a probability-based implementation of the Mowse algorithm. The total score is the absolute probability that the observed match is a random event and is calculated as $-10 \cdot \log_{10}(P)$, where P is the absolute probability. Expect, expectation value, which is directly equivalent to the *E*-value in a BLAST search result. The lower the expectation value, the more significant the score.

Source	Site	Name	M_r(expt)	M_r(calc)	Delta	MC	Score	Expect	Peptide
TiO_2	Thr^4	hupA	1581.3848	1581.7837	-0.3989	1	101	1.40×10^{-8}	-.MNK**pT**QLIDVIAEK.A
IMAC	Thr^{19}	hupA	1054.2634	1054.506	-0.2425	1	30	0.018	K.AELSK**pT**QAK.A
IMAC	Ser^{17}/Thr^{19}	hupA	1134.2084	1134.4723	-0.2638	1	45	0.00029	K.AEL**pS**K**pT**QAK.A
TiO_2	Ser^{27}/Thr^{33}	hupA	1676.3594	1676.7674	-0.4080	0	53	2.40×10^{-5}	K.AALE**pS**TLAAI**pT**ESLK.E
TiO_2	Thr^{28}/Thr^{33}	hupA	1676.3608	1676.7674	-0.4066	0	57	8.90×10^{-6}	K.AALES**pT**LAAI**pT**ESLK.E
TiO_2	Ser^{81}	hupA	1323.3224	1323.6588	-0.3363	0	79	2.00×10^{-7}	K.IAAANVPAFV**pS**GK.A
TiO_2	Ser^4	hupB	1155.2196	1155.5359	-0.3162	1	40	0.016	-.MNK**pS**QLIDK.I
P-bodies	Ser^4	hupB	1024.2108	1024.4954	-0.2845	1	43	0.0008	M.NK**pS**QLIDK.I
TiO_2	Thr^{65}/Thr^{70}	hupB	1600.3228	1600.7263	-0.4034	1	109	7.00×10^{-10}	R.NPQ**pT**GKEI**pT**IAAAK.V
TiO_2	Ser^{21}	groS	1281.3088	1281.6330	-0.3241	0	65	1.80×10^{5}	K.**pS**AGGIVLTGSAAAK.S
TiO_2	Thr^{28}	groS	1281.3080	1281.6330	-0.3249	0	43	0.00041	K.SAGGIVL**pT**GSAAAK.S
TiO_2	Ser^{21}/Thr^{28}	groS	1361.2596	1361.5993	-0.3396	0	89	3.70×10^{-8}	K.**pS**AGGIVL**pT**GSAAAK.S
TiO_2	Ser^{21}/Ser^{30}	groS	1361.2416	1361.5993	-0.3576	0	74	1.70×10^{-6}	K.**pS**AGGIVLTG**pS**AAAK.S
TiO_2	Ser^{28}	lacI	1218.2710	1218.5758	-0.3047	0	47	8.30×10^{5}	R.VVNQA**pS**HVSAK.T
TiO_2	Ser^{28}/Ser^{31}	lacI	1298.1776	1298.5421	-0.3645	0	74	4.20×10^{-7}	R.VVNQA**pS**HV**pS**AK.T
TiO_2	Ser^{28}/Thr^{34}	lacI	1555.2901	1555.6909	-0.4008	1	75	4.40×10^{-7}	R.VVNQA**pS**HVSAK**pT**R.E
TiO_2	Ser^{31}/Thr^{34}	lacI	1555.3120	1555.6909	-0.3789	1	78	7.70×10^{-7}	R.VVNQASHV**pS**AK**pT**R.E
TiO_2	Ser^{28}/Ser^{31}/Thr^{34}	lacI	1635.2568	1635.6572	-0.4004	1	96	6.40×10^{-9}	R.VVNQA**pS**HV**pS**AK**pT**R.E
TiO_2	Ser^{93}/Ser^{97}	lacI	1719.3072	1719.7304	-0.4231	0	49	0.00021	R.ADQLGA**pS**VVV**pS**MVER.S
TiO_2	Thr^{334}	lacI	1436.3126	1436.6661	-0.3534	0	89	7.90×10^{-8}	K.TTLAPN**pT**QTASPR.A
TiO_2	Thr^{328}/Thr^{329}	lacI	1880.3242	1880.7948	-0.4705	2	74	2.20×10^{-7}	K.RK**pT**p**T**LAPN**pT**QTASPR.A
TiO_2	Ser^{345}	lacI	1267.2794	1267.5995	-0.3201	0	78	8.20×10^{-7}	R.ALAD**pS**LMQLAR.Q
TiO_2	Thr^{144}	rpsA	991.1918	991.4376	-0.2457	0	24	0.026	R.D**pT**LHLEGK.E
TiO_2	Ser^{169}	rpsA	866.1780	866.4011	-0.2231	0	35	0.0096	R.NNVVV**pS**R.R
TiO_2	Thr^{455}/Thr^{459}	rpsA	1488.3286	1488.6990	-0.3704	1	98	4.00×10^{-9}	K.GAIV**pT**GKV**pT**AVDAK.G
P-bodies	Thr^2/Ser^4	rpsA	1818.2380	1818.7188	-0.4807	0	45	1.10×10^{-4}	-.M**pT**E**pS**FAQLFEESLK.E
TiO_2	Ser^{73}	rpsI	1122.2354	1122.5183	-0.2828	0	106	6.90×10^{-9}	K.GGGI**pS**GQAGAIR.H
IMAC	Ser^{128}	rpsI	997.2474	997.4858	-0.2384	1	19	0.15	R.RRPQF**pS**K.R
TiO_2	Thr^{20}/Ser^{21}	rpsM	1587.3568	1587.7463	-0.3894	0	95	8.00×10^{-9}	K.HAVIAL**pT**p**S**IYGVGK.T
TiO_2	Ser^{74}/Ser^{76}	rpsM	1278.2396	1278.5556	-0.316	2	46	0.0013	R.REI**pS**M**pS**IKR.L
TiO_2	Ser^{22}/Thr^{24}	rpsE	1486.3968	1486.7673	-0.3705	2	42	0.00069	K.LIAVNRV**pS**K**pT**VK.G
IMAC	Thr^{20}	rpsB	1188.2416	1188.5190	-0.2773	0	67	9.70×10^{-6}	K.AGVHFGHQ**pT**R.Y
TiO_2	Ser^{95}/Thr^{96}	rpsK	1285.1976	1285.5217	-0.3241	1	36	0.0043	K.GPGPGRE**pS**p**T**IR.A
P-bodies	Thr^3/Thr^{10}	rplM	1695.3088	1695.782	-0.4732	2	58	2.50×10^{-5}	-.MK**pT**FTAKPE**pT**VKR.D
TiO_2	Thr^3/Thr^5/Thr^{10}	rplM	1775.2999	1775.7483	-0.4485	2	79	3.40×10^{-7}	-.MK**pT**F**pT**AKPE**pT**VKR.D
TiO_2	Thr^5/Ser^{12}	rplO	1403.2528	1403.6098	-0.3570	1	43	0.00054	R.LN**pT**LSPAEG**pS**KK.A
TiO_2	Ser^{25}/Thr^{30}	rplO	1218.2586	1218.5159	-0.2573	1	5	1.1	R.GIG**pS**GLGK**pT**GGR.G
TiO_2	Ser^{73}	rplE	687.1339	687.2993	-0.1654	0	33	0.046	K.**pS**VAGFK.I
TiO_2	Thr^{63}/Thr^{69}	rplA	1224.2044	1224.5054	-0.3009	0	25	0.0069	R.GA**pT**VLPHG**pT**GR.S
TiO_2	Thr^{51}/Thr^{52}	rplC	1175.2374	1175.5352	-0.2978	1	20	0.013	R.AIQV**pT**p**T**GAKK.A
IMAC	Ser^{19}/Thr^{25}	rpmB	1156.2116	1156.4791	-0.2674	1	64	3.90×10^{-5}	R.**pS**HALNA**pT**KR.R
IMAC	Thr^{14}/Ser^{19}/Thr^{25}	rpmB	2130.4324	2130.9238	-0.4914	2	62	2.00×10^{-6}	R.VPVP**pT**GNNR**pS**HALNA**pT**KR.R
IMAC	Ser^{30}/Thr^{37}/Thr^{39}	rplV	1960.4137	1960.8713	-0.4576	2	51	0.00023	K.KV**pS**QALDIL**pT**Y**pT**NKK.A
TiO_2	Thr^{60}/Thr^{65}	dnaK	1703.3538	1703.7685	-0.4146	0	38	0.00088	R.QAV**pT**NPQN**pT**LFAIK.R
TiO_2	Ser^{453}	dnaK	1677.3844	1677.7876	-0.4031	0	88	1.50×10^{-7}	K.**pS**LGQFNLDGINPAPR.G
TiO_2	Ser^{505}	dnaK	1369.2368	1369.5762	-0.3394	0	67	1.10×10^{-6}	K.AS**pS**GLNEDEIQK.M
TiO_2	Ser^{201}	gapA	1480.3204	1480.6923	-0.3718	0	65	4.30×10^{-6}	R.GA**pS**QNIIPSSTGAAK.A
TiO_2	Ser^{201}/Ser^{207}	gapA	1560.2696	1560.6586	-0.3889	0	39	0.00055	R.GA**pS**QNIIP**pS**STGAAK.A
P-bodies	Ser^{201}/Thr^{209}	gapA	1560.2372	1560.6586	-0.4213	0	38	0.0011	R.GA**pS**QNIIPSS**pT**GAAK.A
TiO_2	Ser^{239}/Thr^{244}	gapA	1654.3610	1654.7733	-0.4122	0	119	1.20×10^{-10}	R.VPTPNV**pS**VVDL**pT**VR.L
IMAC	Ser^{190}	gapA	1376.2531	1376.5874	-0.3344	1	77	2.80×10^{-7}	K.TVDGP**pS**HKDWR.G
TiO_2	Thr^{544}/Thr^{552}	rpoD	1454.2760	1454.6320	-0.3559	0	62	2.10×10^{-6}	R.AA**pT**HDVLAGL**pT**AR.E
TiO_2	Ser^{602}/Ser^{604}	rpoD	1239.2252	1239.5162	-0.2910	1	29	0.0058	R.HP**pS**R**pS**EVLR.S
TiO_2	Thr^{67}/Thr^{74}	ihfA	1570.2908	1570.6793	-0.3885	1	103	5.00×10^{-10}	R.NPK**pT**GEDIPI**pT**AR.R
TiO_2	Thr^{66}	ihfB	1154.2326	1154.5220	-0.2894	1	60	5.60×10^{-5}	K.**pT**GDKVELEGK.Y
TiO_2	Ser^{72}	tig	1212.2142	1212.5210	-0.3067	0	90	2.90×10^{-7}	R.QDVLGDLM**pS**R.N
TiO_2	Ser^9	crr	1211.3148	1211.6162	-0.3014	2	65	1.00×10^{-5}	K.LK**pS**LVSDDKK.D
TiO_2	Ser^9/Ser^{12}	crr	1291.2638	1291.5826	-0.3187	2	51	0.00038	K.LK**pS**LV**pS**DDKK.D
TiO_2	Ser^2/Thr^6	cspA	1079.1738	1079.4487	-0.2749	1	43	0.0017	M.**pS**GKM**pT**GIVK.W
TiO_2	Thr^{324}/Thr^{327}	ftsZ	1329.2768	1329.6095	-0.3326	0	67	1.60×10^{-6}	K.RPEI**pT**LV**pT**NK.Q
TiO_2	Thr^{71}/Thr^{78}	tatA	1991.2990	1991.7986	-0.4997	2	60	8.70×10^{-5}	K.QAD**pT**NQEQAK**pT**EDAKR.H
TiO_2	Ser^{54}/Thr^{60}	infB	1387.2484	1387.5898	-0.3413	1	54	0.0001	K.N**pS**GPDKL**pT**LQR.K
TiO_2	Ser^9/Thr^{14}	accD	1188.2380	1188.5305	-0.2924	1	52	0.00042	R.IK**pS**NITP**pT**R.K

Table S1   Continued

Source	Site	Name	M_r(expt)	M_r(calc)	Delta	MC	Score	Expect	Peptide
TiO$_2$	Thr^3	gatZ	911.2322	911.4663	− 0.2341	1	46	0.0025	-.MK**pT**LIAR.H
TiO$_2$	Ser^{476}	aspA	1106.1322	1106.3917	− 0.2595	1	45	0.0017	K.RYTDE**pS**EQ.-
TiO$_2$	Thr^{626}/Thr^{630}	pnp	1082.1788	1082.4563	− 0.2774	1	36	0.0098	R.VY**pT**GKV**pT**R.I
TiO$_2$	Ser^3/Thr^8	gatD	1592.2680	1592.6671	− 0.3990	1	41	0.00036	-.MK**pS**VVND**pT**DGIVR.V
TiO$_2$	Thr^{87}/Thr^{97}	sucB	1878.3088	1878.7761	− 0.4673	2	40	0.0014	K.E**pT**SAKSEEKAS**pT**PAQR.Q
TiO$_2$	Ser^{75}	frr	927.1428	927.3773	− 0.2344	0	39	0.0078	R.SM**pS**PAVEK.A
TiO$_2$	Ser^2	lipA	1038.2284	1038.4933	− 0.2648	0	30	0.019	M.**pS**KPIVMER.G
IMAC	Thr^6	yqjD	1316.2666	1316.5874	− 0.3208	1	54	5.00×10^{-5}	M.SKEH**pT**TEHLR.A
IMAC	Thr^7	yqjD	1316.2684	1316.5874	− 0.3190	1	33	0.0047	M.SKEHT**pT**EHLR.A
IMAC	Thr^6/Thr^7	yqjD	1396.2338	1396.5537	− 0.3199	1	67	5.80×10^{-6}	M.SKEH**pTpT**EHLR.A
IMAC	Thr^{17}	espF	921.2758	921.4069	− 0.1311	0	29	0.026	R.HI**pT**SAASR.V
IMAC	Thr^{76}	grpE	1238.3146	1238.6020	− 0.2873	2	28	0.039	R.RR**pT**ELDIEK.A
IMAC	Thr^{94}	tufA	2736.8350	2737.2639	− 0.4289	0	25	0.024	K.NMI**pT**GAAGMDGAILVVAATDGPMPQTR.E
P-bodies	Thr^{176}/Ser^{180}	ahpC	1658.2694	1658.7205	− 0.4511	0	35	0.0025	K.EGEA**pT**LAP**pS**LDLVGK.I

REFERENCE

1   Oh, M.-H., Ray, W. K., Huber, S. C., Asara, J. M., Gage, D. A. and Clouse, S. D. (2000) Recombinant brassinosteroid insensitive 1 receptor-like kinase autophosphorylates on serine and threonine residues and phosphorylates a conserved peptide motif *in vitro*. Plant Physiol. **124**, 751–766